

NOTICE: this is the author's version of a work that was accepted for publication in the journal Computerized Medical Imaging and Graphics. Changes resulting from the publishing process, such as peer review, editing, corrections, structural formatting, and other quality control mechanisms may not be reflected in this document. Changes may have been made to this work since it was submitted for publication. A definitive version was subsequently published in the Journal Computerized Medical Imaging and Graphics, Vol.37, No.3 (2013). DOI: [10.1016/j.compmedimag.2013.02.001](https://doi.org/10.1016/j.compmedimag.2013.02.001).

## **Hemodynamic analysis of the effect of different types of plaque in the left coronary artery**

Thanapong Chaichana<sup>1</sup>, Zhonghua Sun<sup>1</sup>, James Jewkes<sup>2</sup>

1. Discipline of Medical Imaging, Department of Imaging and Applied Physics, Curtin University, Perth, Western Australia, Australia, 6845

2. Fluid Dynamics Research Group, Department of Mechanical Engineering, Curtin University, Perth, Western Australia, Australia, 6845

### **Corresponding author:**

Associate Professor Zhonghua Sun, Discipline of Medical Imaging, Department of Imaging and Applied Physics, Curtin University, GPO Box, U1987, Perth, Western Australia 6845, Australia

Tel: +61-8-9266 7509

Fax: +61-8-9266 2377

Email: [z.sun@curtin.edu.au](mailto:z.sun@curtin.edu.au)

## **Abstract**

**Purpose:** Coronary plaque has been shown to directly affect the blood parameters, however, hemodynamic variations based on the plaque configuration has not been studied. In this study we investigate the hemodynamic effects of various types of plaque in the left coronary bifurcation.

**Methods:** Eight types of plaque configurations were simulated and located in various positions in the left main stem, the left anterior descending and left circumflex to produce a >50% narrowing of the coronary lumen. We analyse and characterise hemodynamic effects caused by each type of plaque. Computational fluid dynamics was performed to simulate realistic physiological conditions that reveal the *in vivo* cardiac hemodynamics. Velocity, wall shear stress (WSS) and pressure gradient (PSG) in the left coronary artery were calculated and compared in all plaque configurations during cardiac cycles.

**Results:** Our results showed that the highest velocity and PSG were found in the type of plaque configuration which involved all of the three left coronary branches. Plaques located in the left circumflex branch resulted in highly significant changes of the velocity, WSS and PSG ( $p < 0.001$ ) when compared to the other types of plaque configurations.

**Conclusion:** Our analysis provides an insight into the distribution of plaque at the left bifurcation, and corresponding hemodynamic effects, thus, improving our understanding of atherosclerosis.

**Keywords:** computational fluid dynamics, plaque, pressure gradient, hemodynamic, coronary bifurcation

## **Introduction**

The angulation of the left coronary bifurcation has an effect upon blood flow that might lead to the development of atherosclerotic plaque. A recent study has shown that wide angulations can significantly increase disturbances to the flow field that are associated with the progression of coronary plaque [1]. Plaques most commonly originate in the left coronary bifurcation [2]. Various types of bifurcation plaque lesions have been classified by Topol [3], with special attention paid to the important distinction between a true bifurcation (consisting of the main branch and the side branch) and a pseudo bifurcation (which includes all of the other lesions involving a bifurcation). These distinctions are a key element in the proper planning of treatment. Cases with a lumen narrowing of  $>50\%$  were considered hemodynamically significant [3], since this level of narrowing results in significant hemodynamic changes to the flow within the coronary artery [4]. Previous studies used computational fluid dynamics (CFD) to investigate the hemodynamic changes due to the severity of stenosis [5, 6]. The results of those studies confirmed that a stenosis of  $<50\%$  coronary diameter due to plaque formation has a minimal effect on the flow-field inside the coronary artery.

Recent studies on the effect of plaque distributed in the left coronary bifurcation have shown that there is a direct effect on the flow parameters at stenotic locations [7-9]. It is important for us to understand the hemodynamic patterns corresponding to the types of bifurcation plaque, since the different plaque positions may lead to various hemodynamic effects, although this has not been systematically studied. To the best of our knowledge, there are no publications related to the investigation of hemodynamic variations based on the classification of plaque configurations. Thus, this work aims to study the

hemodynamic changes due to the different types of bifurcation plaque (Fig. 1), based on realistic coronary models. It is expected that the research findings will provide potential value for improving our understanding of the flow field induced by these various bifurcation plaques, and contribute to our understanding of the pathogenesis of coronary artery disease.

## **Material and Methods**

### *Patient information and left coronary artery geometry*

A 47-year-old male with suspected coronary artery disease (CAD) was selected in this study to provide the realistic left coronary geometry, including its side branches. The patient's CT volume data was used to create left coronary artery (LCA) geometry. Image segmentation and post-processing techniques were performed using Analyze 7.0 (Analyze Direct, Inc., Lexana, KS, USA). The CT scan was performed with a 64-slice scanner (GE Medical Systems, Lightspeed VCT, 64x0.625 mm) with the following protocols: beam collimation 0.625 mm, pitch 0.2-0.26, reconstruction interval of 0.4 mm, with tube voltage of 120 kVp and tube current ranging from 300 to 650 mAs. Axial images were reconstructed with a slice thickness of 0.625 mm in 0.4 mm increments, resulting in isotropic volume data with a voxel size of 0.4 x 0.4 x 0.4 mm<sup>3</sup>. Scan-related artefacts and unwanted soft tissues were manually removed in 2D axial slices [10, 11]. Fig. 2 demonstrates the realistic LCA model and the rectangle box refers to the effective plaque locations (EPLs). EPL represents the flow changes in the LCA surrounding the plaque locations. LCA geometry was created for the various EPLs in the left main bifurcation, consisting of the left main stem (LMS), left anterior descending (LAD), left circumflex (LCx), and its side branches. Dimensions of the LCA geometry were

measured and shown in Table 1. The geometry of the arteries around the LMS, LAD and LCx was obtained from the sample patient with suspected CAD (plaque type F as shown in Fig. 1). LCA surface geometry, comprising of plaque and normal coronary arteries, were changed into solid models and saved in 'STL format' for the computational meshing procedure.

#### *Various plaque positions in the left coronary bifurcation*

Calcified plaque was generated at different anatomical locations in the left bifurcation, as shown in Fig. 1. This is based on the bifurcation lesions reported in previous studies [3, 12]. There were eight plaque configurations simulated altogether, with a type F plaque being the first model, based directly upon the selected patient's anatomical structures. The other seven types were subsequently adapted from this configuration. Fig. 3 shows the eight different configurations of realistic plaques were generated to study the flow effects. The geometry of the type F plaques at the LCx shows that the dimensions of each section were 1.14 mm in height, a mean width of 3.76 mm and a thickness of 1.46 mm and 1.53 mm (from left to right in Fig. 3). In addition, the geometry of other types of plaques at the LAD branches comprised of two sections, 1.17 mm in height, a mean width of 3.59 mm and a thickness of 1.38 mm and 1.56 mm (from left to right in Fig. 3). Although plaques contain different components depending on the concentration of calcium and lipid materials [13], only hard plaque (calcified plaque) was simulated in this study since this type of plaque is commonly seen in patients with coronary artery disease, and calcified plaque indicates the atherosclerotic changes to the coronary wall, leading to significant stenosis. The simulation of hard plaque is suitable for demonstrating the hemodynamic changes at the EPL in this study. Finally, the diseased condition was

simulated with the generation of eight models with various types of bifurcation plaques, and one baseline model without the presence of plaque is also simulated. There were nine LCA geometries in total.

### *Computational flow and solution*

The STL models were divided into LCA geometry and plaque sections, and plaque models were merged with the LCA models in the various location combinations. These combined STLs were then used to create a volume mesh using the ANSYS ICEM CFD hexahedral meshing tool with details having been described in previous studies [1, 14, 15]. Mesh resolution for the various models ranged from  $9 \times 10^5$  to  $9.8 \times 10^5$  cells. The baseline LCA geometry model (without plaques) was created using the same process, yielding  $9.5 \times 10^5$  cells. A mesh independence case was produced and solved for this baseline model at approximately twice the resolution; this demonstrated agreement with the lower resolution mesh applied in this study. Mesh convergence was established by re-running a test simulation at double the quoted grid resolution, and looking for discrepancies in the solution. It was found that mesh convergence had been achieved, and the fairly fine meshes described above were acceptable for the purposes of this study.

The pulsatile flow rates and pressure at the aorta and LCA were reconstructed using a Fourier series in Matlab (MathWorks, Inc. Natick, MA, USA) [16, 17]. The transient simulation was performed using accurate hemodynamic rheological and material properties, as described in a previous study [18]. Pulsatile velocity (Fig. 4a) was applied as an inflow boundary condition at the left main stem [5, 19]. The Reynolds number of inlet blood flow was found to match for the experiments.

The outflow boundary condition was applied with the flow ratio through the six side-branches (Fig. 2) at the LAD (SB1, 2 and 3) and LCx (SB4, 5 and 6) according to side-branches diameters (Table 1) [20, 21]. The outflow relationship is also known as Murray's law and the summation of outflow conditions through the side-branches is equal to the flow at the inlet [22]. Rheological parameters were applied with a blood density of 1060 kg/m<sup>3</sup>, blood viscosity of 0.0035 Pa s [23, 24]. Plaques and blood-vessels were assumed to be rigid [25]. Blood flow was assumed to be laminar. A no-slip condition was applied at the walls [26]. The blood was assumed to be Newtonian and incompressible [27, 28]. The Navier-Stokes equations were solved using the ANSYS CFX CFD package (version 12 - ANSYS, Inc.), on a Microsoft Windows 7 32-bit machine, 6 GB of RAM with a Xeon W3505 2.53 GHz CPU. The CFD simulation was run for 64 time-steps, representing 0.8s of phasic coronary blood flow rate (0.0125s per time-step). The CFD simulation was converged to a residual target of less than 1×10<sup>-4</sup> per time-step in each LCA model. ANSYS CFD-Post version 12 (ANSYS, Inc.) was used to calculate and visualise flow velocity, pressure gradient (PSG) and wall shear stress (WSS).

The PSG is calculated from the local static pressure, to characterise the high amplitude pressure changes at the EPL. The static pressure at stenotic locations is similar to the pressure at the coronary inlet and is poorly suited to the classification of the pressure effects [29]. The PSG is defined as:

$$\text{PSG} = \sqrt{\left(\frac{\partial p}{\partial u}\right)^2 + \left(\frac{\partial p}{\partial v}\right)^2 + \left(\frac{\partial p}{\partial w}\right)^2} \quad (1)$$

where  $p$  is local static pressure in the area of interest  $u$ ,  $v$ , and  $w$  and are points in the Cartesian  $x$ ,  $y$ , and  $z$  coordinates. PSG has been shown to be a significant indicator of coronary disease [29, 30].

The WSS is a commonly used parameter in hemodynamic analysis; endothelial cells have been shown to align themselves with the flow direction that corresponds to the local WSS. The coordinates of the wall surface elucidate the interaction of instantaneous WSS vectors and endothelial cells [31].

$$WSS = \frac{1}{T} \int_0^T \left| \mu \frac{\partial v_t}{\partial n} \right| dt \quad (2)$$

where  $\mu$  is blood viscosity,  $v_t$  is velocity vector near wall perpendicular to surface and  $n$  is distance to the wall surface,  $T$  is pulsatile period,  $dt$  is the time derivative of the local shear stress. The quantitative parameters used to characterise the impact of plaques on coronary side branches is local WSS magnitude, and this has been demonstrated in our previous study [8].

#### *Statistical analysis of hemodynamic parameters*

Hemodynamic parameters were exported in “CSV format” from ANSYS CFD-Post version 12 (ANSYS, Inc.). The WSS, PSG and velocity were entered into SPSS 17.0 (SPSS, Inc., Chicago, IL, USA) for statistical analysis. A p-value of <0.05 was considered to indicate statistically significant differences. A one way Analysis of Variance (ANOVA) between groups with post-hoc comparisons was used for analysis of hemodynamic factors to determine the differences among the eight types of bifurcation plaque.

## Results

### *Comparison of hemodynamic parameters*

There were significant differences in the majority of hemodynamic factors (WSS, PSG and velocity) between comparisons of the eight different bifurcation plaques as tested with one way ANOVA ( $p < 0.05$ ). However, there was no significant difference in WSS and PSG parameters between type A and type B and type C ( $p > 0.05$ ). Similarly, no significant differences were found in WSS and PSG between type F, and types A, B and C ( $p > 0.05$ ). For the comparisons between the remaining types, most of them demonstrated significant differences.

### *Comparison of cross-sectional velocity*

Fifteen cross-sections were defined, as shown in Fig. 4b, with the type D plaque shown as an example. Contours of axial velocities have been plotted on 15 equally spaced lines normal to the flow direction. The contour plots of axial velocities and streamlines traces in the coronary models were presented after extraction of the flow information within the anatomical geometry. These cross-sections were applied to the other seven plaque configurations and to the baseline as well. The cross-sections were divided into three groups, with each group having five sectional-planes: sections A-E at the LMS, sections F-J at the LAD and sections K-O at the LCx respectively. Table 2 shows the comparisons of cross-sectional averaged velocity at the EPL for the eight bifurcation plaques. In the systolic phase, type A has the two sections of plaque-intersection (PIN) (✓) at sections C and E, and one section of the exclusive plaque-intersection (EPIN) (✓✓) at section D. In addition, a high average velocity in section D was reached, from  $11.04 \text{ mm s}^{-1}$  to  $11.77 \text{ mm s}^{-1}$  as shown in types A, C, D and F, and there is a minimal velocity change when

compared to the normal velocity, which reached  $8.90 \text{ mm s}^{-1}$ . Section G in the types B, D, E, F and H was the EPIN with velocity ranging from  $11.43 \text{ mm s}^{-1}$  to  $13.61 \text{ mm s}^{-1}$ , showing extremely high average velocity when compared to the normal velocity, which is  $4.13 \text{ mm s}^{-1}$ . Furthermore, section L in the types B, C, D and G was also the EPIN with velocity ranging from  $17.84 \text{ mm s}^{-1}$  to  $19.82 \text{ mm s}^{-1}$ , demonstrating extremely high average velocity when compared to the normal velocity, which is  $5.18 \text{ mm s}^{-1}$ . The type H configuration was found to have very similar average cross-sectional velocity values in both systolic and diastolic phases, to those observed during the normal flow condition. Similar results were noticed in the diastolic phase for the comparisons of average cross-sectional velocity, except for type G, which shows apparently high average velocity in all sections when compared to other types of plaque configurations.

#### *Velocity inside the left coronary artery*

To characterise the hemodynamic variations of different types of plaques at the left coronary artery, velocity patterns were calculated and compared in all eight types of bifurcation plaque and the baseline, as shown in Fig. 5 and 6. The plots were chosen to reveal the flow effects at the EPL. The velocity patterns were calculated and visualised at a systolic phase of  $0.2 \text{ s}$  (Fig. 5) and the diastolic phase of  $0.7 \text{ s}$  (Fig. 6). The velocity values ranged from  $0 \text{ mm s}^{-1}$  to  $30.50 \text{ mm s}^{-1}$ , corresponding to fifteen contour levels, approximately  $2.03 \text{ mm s}^{-1}$  at per level. Fig. 5 shows high velocity in the red and yellow contour levels, which ranged from  $28.23 \text{ mm s}^{-1}$  to  $30.50 \text{ mm s}^{-1}$  at the stenotic locations (specifically in types A, C and G, as these types had plaques at the LMS and LCx branches). In addition, the bifurcation plaques involving the LMS and LAD branches (especially for types E, F and H) show high velocity regions at LMS branch and the LAD

branch (stenotic positions), ranging from  $21.79 \text{ mm s}^{-1}$  to  $23.98 \text{ mm s}^{-1}$ . Type B had the bifurcation plaques located in the LAD and LCx branches, and high velocity was observed at the LCx, and the LAD around the stenotic regions. Type D has the bifurcation plaque positioned in LMS, LAD and LCx branches, and it generated similar flow effects to the other types, with the high velocity regions near plaque locations at the LMS and LCx branches, and the LAD branch. Fig. 6 shows the flow in the systolic phase, however, there are more regions of high velocity in the stenotic locations at LMS, LAD and LCx branches. Thus, the recirculation regions were found downstream of plaque locations in all types of bifurcation plaques and in both systolic and diastolic phases.

#### *Pressure gradient in the left coronary artery*

PSG was calculated at the systolic phase of 0.2 s and diastolic phase of 0.7 s, and was displayed within the coronary artery at EPL in order to compare the PSG changes for all eight models. PSG values ranged from  $-15 \text{ kg/m}^2 \text{ s}^2$  to  $500 \text{ kg/m}^2 \text{ s}^2$ , corresponding to 15 contour levels. Fig. 7 reveals PSG variations with the bifurcation plaques and normal condition during the diastolic phase (0.7 s). The high PSG was found in all types of bifurcation plaques at the stenotic locations, with values ranging from  $463.21 \text{ kg/m}^2 \text{ s}^2$  to  $500.00 \text{ kg/m}^2 \text{ s}^2$ . Large distribution of high PSG was found in the type D configuration. The high PSG was also found at post-plaque locations, and this was particularly apparent in types A, C, D and F. The type G was found to be different from the other types in terms of PSG changes due to only the involvement of the LCx, and this is consistent with the statistical comparisons (type G had significantly different PSG changes when compared to the other types). Fig. 8 reveals the comparison of PSG in all types of bifurcation plaque configurations with the baseline, during the systolic phase (0.2 s). The

high PSG at stenotic locations ranged  $352.86 \text{ kg/m}^2 \text{ s}^2$  to  $389.64 \text{ kg/m}^2 \text{ s}^2$ . Thus, PSG variations were distributed in the same pattern as that observed in the diastolic phase (Fig. 7).

## **Discussion**

This study reveals that the various types of bifurcation plaques influence the subsequent hemodynamic parameters in the left coronary bifurcation, resulting in flow changes. This finding provides additional information about the hemodynamic effect of coronary plaque; hence, it improves our understanding of the atherosclerotic changes due to the presence of plaques at different coronary locations.

The classification system was considered to be a practical way of dealing with the various bifurcation lesions, allowing us to make distinctions between the various bifurcation geometries [3]. In this study, we investigated the hemodynamic effects of these plaques, and determined whether there exists a statistically significant difference in variable parameters. To the best of our knowledge, this is the first study to present information on different types of plaques in the left coronary artery with investigation of corresponding hemodynamic effect. Our results showed that types A, G and H (plaque located in each LMS, LCx and LAD branches) lead to less severe hemodynamic variations around the bifurcation than the other types (B, C, D, E and F). In addition, type D produces more significant flow variations at the coronary bifurcation than the other seven types of bifurcation plaque. These findings provide an insight into the effect of plaque position upon subsequent hemodynamics in the left coronary artery.

Coronary plaque generally originates in the bifurcation region due to the angulations. The angulations cause a region of low WSS, as confirmed by our study and previous reports [1-4, 32-34]. Medical imaging modality such as intravascular ultrasound and multislice CT coronary angiography has been commonly used to detect plaque locations in the left main coronary artery [14, 35-37]. These imaging techniques provide valuable diagnostic information, such as assessment of plaque components and corresponding coronary lumen changes, however, they offer no tangible insight into the resultant hemodynamics. Computational fluid dynamics provides an opportunity to predict the hemodynamic behaviour [1, 31, 38]. Thus, the characterisation of hemodynamic variations due to the various types of bifurcation plaque in the configurations can be further explored with flow visualisations; this exceeds the classical anatomical analysis of coronary stenosis or occlusion.

This study visualised the wall shear stress, velocity and pressure gradient inside the left coronary bifurcations, and compared the hemodynamic parameters between different bifurcation plaques statistically. We found that plaque type G was very different from the other types. Types D and H were found to produce different velocity, WSS and PSG distributions compared to the other types. Types A, B, C and F were very similar in velocity, WSS and PSG, compared to the plaque types D, E, F and H. Type E was found to have PSG similar to that observed in other types. Our results indicate that different types of plaque demonstrate various hemodynamic effects, although most of the types are statistically significantly different from the other types, as shown in table 2. Some types of plaques caused unique effects, for example, type D resulting in huge velocity variations. Type A showed limited velocity variations compared to the baseline. Thus, it

is clinically important to understand the different types of plaques and their corresponding hemodynamic effects.

Wall shear stress has been confirmed to be closely associated with the development of atherosclerosis. It has been revealed that atherogenesis preferentially involves the outer walls of vessel bifurcations, side branches and regions of high curvature in the arterial tree [32, 39]. In these geometrically predisposed locations where circulating atherogenic blood particles tend to increase, WSS is significantly lower in magnitude and demonstrates directional changes and flow separation. On the other hand, these blood particles are washed away from regions due to high WSS caused by severe stenosis, and decreases intercellular permeability, consequently increases the vulnerability of these regions leading to plaque rupture. Our results showed that WSS was significantly increased in the presence of different types of plaques, with disturbances in the physiological pattern of blood flow noted in the post-stenotic regions. This in turn results in WSS alterations [40, 41]. Thus, our analysis provides insight into the complex hemodynamic effects caused by different types of plaques at the coronary artery branches.

In the clinical situation, the PSG magnitude has been used to assess the severity of plaques and characterise the impacts of plaque in the left main coronary bifurcation [42, 43]. The highest PSG region may indicate the location of a potential coronary plaque rupture. The type D configuration shows the largest distribution of high PSG at the bifurcation, thus, this type is potentially more dangerous than the other types during the diastolic phase (Fig. 7). The hemodynamic factors were shown as velocity patterns and PSG, for the analysis of changes inside the coronary artery at the main bifurcation. WSS

was analysed in this study, however it was not shown visually and was only used for the statistical analysis.

There are some limitations in this study that should be addressed. Firstly, the blood model was assumed to have a Newtonian viscosity. Our study focused on the hemodynamic visualisation of the coronary artery and this assumption has been shown to be reasonable by previous studies [27, 44]. Secondly, realistic LCA geometries were assumed to have a rigid wall rather than an elastic wall; hence, the simulation does not completely reflect the realistic physiological behaviour, as the coronary wall is moving during cardiac cycles. Thirdly, the same inlet flow waveform was applied to all types of plaque configurations, which could affect the results to some extent. Due to different locations of simulated plaques at the left coronary artery branches, it is likely that hemodynamic changes could be affected by various plaque configurations or plaque severity leading to the pressure difference and pressure drop. Thus, application of different flow waveforms corresponding to the different anatomical regions of coronary artery is suggested with aim of generating more realistic results. Finally, a single patient has been selected for the generation of various bifurcation plaques and coronary models. Only the left main, LAD and LCx branches were included in the models, while side branches were removed. Although this study focused on the hemodynamic effects of bifurcation plaques, removal of secondary flows and other important flow structures could change the hemodynamic quantities such as WSS [45]. Despite this limitation, the simulated models represent realistic coronary geometry, and accordingly, our results are still valid for clinical applications. Future studies will analyse realistic plaque at the

bifurcation based on different patients' data and different configurations (concentric versus eccentric plaques).

In conclusion, this study investigates the different types of bifurcation plaques in the realistic left coronary artery and visualises the velocity patterns and PSG variations within left coronary bifurcation. Statistical analysis has been performed to compare the hemodynamic factors for characterisation of various plaques at bifurcation regions. Significant differences are noticed in the hemodynamic parameters among these type configurations. Velocity and PSG are increased when the left coronary bifurcation contains more plaques, and this is especially apparent with type of simulation involving all of the left coronary branches. The research findings of this study indicate that extra plaque located in left coronary bifurcation may increase the risk of plaque rupture.

**Acknowledgements:** We would like to acknowledge the financial support (PhD scholarship) provided by the State Centre of Excellence in e-Medicine, Department of Commerce, Western Australia, Australia.

## References

1. Chaichana T, Sun Z, Jewkes J. Computation of haemodynamics in the left coronary artery with variable angulations. *J Biomech* 2011; 44(10):1869-1878.
2. Sun Z, Cao Y. Multislice CT angiography assessment of left coronary artery: Correlation between bifurcation angle and dimensions and development of coronary artery disease. *Eur J Radiol* 2011; 79(2):e90-e95.
3. Topol EJ. *Textbook of interventional cardiology*, 5th ed. Philadelphia: Saunders Elsevier, 2008:1075.
4. Fuster V, Lewis A. Conner memorial lecture. Mechanisms leading to myocardial infarction: insights from studies of vascular biology. *Circulation* 1994; 90(4):2126-2146.
5. Katriasis DG, Theodorakakos A, Pantos I, Andriotis A, Efsthopoulos EP, Siontis G, et al. Vortex formation and recirculation zones in left anterior descending artery stenosis: computational fluid dynamics analysis. *Phys Med Biol* 2010; 55(5):1395-1411.
6. Shanmugavelayudam SK, Rubenstein DA, Yin W. Effect of geometrical assumptions on numerical modelling of coronary blood flow under normal and disease conditions. *J Biomech Eng* 2010; 132(6):061004.
7. Chaichana T, Sun Z, Jewkes J. Investigation of the haemodynamic environment of bifurcation plaques within the left coronary artery in realistic patient models based on CT images. *Australas Phys Eng Sci Med* 2012; 35: 232-236.

8. Chaichana T, Sun Z, Jewkes J. Impact of plaques in the left coronary artery on wall shear stress and pressure gradient in coronary side branches. *Comput Methods Biomech Biomed Engin* 2012; DOI: 10.1080/10255842.2012.671308.
9. Chaichana T, Sun Z, Jewkes J. Computational fluid dynamics analysis of the effect of plaque in the left coronary artery. *Comput Math Methods Med* 2012; 2012:504367.
10. Sun Z, Winder RJ, Kelly BE, Ellis PK, Kennedy PT, Hirst DG. Diagnostic value of CT virtual intravascular endoscopy in aortic stent grafting. *J Endovasc Ther* 2004; 11(1):13-25.
11. Sun Z, Winder RJ, Kelly BE, Ellis PK, Hirst DG. CT virtual intravascular endoscopy of abdominal aortic aneurysms treated with suprarenal endovascular stent grafting. *Abdom Imaging* 2003; 28(4):580-587.
12. Enrico B, Suranyi P, Thilo C, et al. Coronary artery plaque formation at coronary CT angiography: morphological analysis and relationship to hemodynamics. *Eur Radiol* 2009; 19: 837-844.
13. Sun Z, Dimpudus FJ, Nugroho J, Adipranoto JD. CT virtual intravascular endoscopy assessment of coronary artery plaque: A preliminary study. *Eur J Radiol* 2010; 75(1):e112-e119.
14. Sun Z, Chaichana T. Fenestrated stent graft repair of abdominal aortic aneurysm: hemodynamic analysis of the effect of fenestrated stents on the renal arteries. *Korean J Radiol* 2010; 11(1):95-106.

15. Sun Z, Chaichana T. Investigation of the hemodynamic effect of stent wires on renal arteries in patients with abdominal aortic aneurysms treated with suprarenal stent-grafts. *Cardiovasc Intervent Radiol* 2009; 32(4):647-657.
16. Nichols WW, O'Rourke MF. McDonald's Blood Flow in Arteries, fifth ed. London: Hodder Arnold, 2005, 326-327.
17. Smith SW. The scientist and engineer's guide to digital signal processing. California Technical Publishing, California, 1997, 255-256.
18. Frauenfelder T, Lotfey M, Boehm T, Wildermuth S. Computational fluid dynamics: hemodynamic changes in abdominal aortic aneurysm after stent-graft implantation. *Cardiovasc Intervent Radiol* 2006; 29 (4), 613-623.
19. Berne RM, Levy MN. Cardiovascular physiology. St Louis MI: Mosby, 2001:231.
20. Giannoglou GD, Soulis JV, Farmakis TM, Giannakoulas GA, Parcharidis GE, Louridas GE. Wall pressure gradient in normal left coronary artery tree. *Med Eng Phys* 2005; 27(6):455-564.
21. van der Giessen AG, Groen HC, Doriot PA, et al. The influence of boundary conditions on wall shear stress distribution in patients specific coronary trees. *J Biomech* 2011; 44(6):1089-1095.
22. Murray CD. The Physiological Principle of Minimum Work: I. The Vascular system and the cost of blood volume. *Proc Natl Acad Sci U S A* 1926; 12(3):207-214.

23. Boutsianis E, Dave H, Frauenfelder T, et al. Computational simulation of intracoronary flow based on real coronary geometry. *Eur J Cardiothorac Surg* 2004; 26(2):248-256.
24. Milnor W. *Hemodynamics*. Baltimore: Williams & Wilkins, 1989.
25. Sun Z, Mwilpatayi B, Chaichana T, Ng C. Hemodynamic effect of calcified plaque on blood flow in carotid artery disease: a preliminary study. *Conf Proc IEEE Bioinfo Biomed Eng* 2009; 1:1-4.
26. Moore JE Jr, Xu C, Glagov S, Zarins CK, Ku DN. Fluid wall shear stress measurements in a model of the human abdominal aorta: oscillatory behavior and relationship to atherosclerosis. *Atherosclerosis* 1994; 110(2):225-240.
27. Johnston BM, Johnston PR, Corney S, Kilpatrick D. Non-Newtonian blood flow in human right coronary arteries: steady state simulations. *J Biomech* 2004; 37(5):709-720.
28. Borghi A, Wood NB, Mohiaddin RH, Xu XY. Fluid-solid interaction simulation of flow and stress pattern in thoracoabdominal aneurysms: a patient-specific study. *J Fluid Struct* 2008; 24:270-280.
29. Garcia D, Kadem L, Savéry D, Pibarot P, Durand LG. Analytical modeling of the instantaneous maximal transvalvular pressure gradient in aortic stenosis. *J Biomech* 2006; 39(16):3036-3044.
30. Garcia D, Pibarot P, Louis-Gilles D. Analytical modeling of the instantaneous pressure gradient across the aortic valve. *J Biomech* 2005; 38(6):1303-1311.

31. Kleinstreuer C, Hyun S, Buchanan JR Jr, Longest PW, Archie JP Jr, Truskey GA. Hemodynamic parameters and early intimal thickening in branching blood vessels. *Crit Rev Biomed Eng* 2001; 29(1):1-64.
32. Asakura T, Karino T. Flow patterns and spatial distribution of atherosclerotic lesions in human coronary arteries. *Circ Res* 1990; 66:1045-1066.
33. Gziut AI. Comparative analysis of atherosclerotic plaque distribution in the left main coronary artery and proximal segments of left anterior descending and left circumflex arteries in patients qualified for percutaneous coronary angioplasty. *Ann Acad Med Stetin* 2006; 52(2):51-62.
34. Han SH, Puma J, García-García HM, et al. Tissue characterisation of atherosclerotic plaque in coronary artery bifurcations: an intravascular ultrasound radiofrequency data analysis in humans. *EuroIntervention* 2010; 6(3):313-320.
35. Gijzen FJ, Wentzel JJ, Thury A, et al. A new imaging technique to study 3-D plaque and shear stress distribution in human coronary artery bifurcations in vivo. *J Biomech* 2007; 40(11), 2349-2357.
36. Grayburn PA, Willard JE, Haagen DR, Brickner ME, Alvarez LG, Eichhorn EJ. Measurement of coronary flow using high-frequency intravascular ultrasound imaging and pulsed Doppler velocimetry: in vitro feasibility studies. *J Am Soc Echocardiogr* 19925(1):5-12.
37. Rodriguez-Granillo GA, Rosales MA, Degrossi E, Durbano I, Rodriguez AE. Multislice CT coronary angiography for the detection of burden, morphology and distribution of atherosclerotic plaque in the left main bifurcation. *Int J Cardiovasc Imaging* 2007; 23(3):389-392.

38. He X, Ku DN. Flow in T-bifurcations: effect of the sharpness of the flow divider. *Biorheology* 1995; 32(4):447-458.
39. Resnick N, Yahav H, Shay-Salit A, et al. Flow shear stress and the vascular endothelium: for better and for worse. *Prog Biophys Mol Biol* 2003; 81: 177-199.
40. Ravensbergen J, Ravensbergen JW, Krijger JK, Hillen B, Hoogstraten HW. Localizing role of hemodynamics in atherosclerosis in several human vertebrobasilar junction geometrics. *Arterioscler Thromb Vasc Biol* 1998; 18: 708-716.
41. Butcher JT, Tressel S, Johnson T, et al. Transcriptional profiles of valvular and vascular endothelial cells reveal phenotypic differences: influence of shear stress. *Arterioscler Thromb Vasc Biol* 2006; 26: 69-77.
42. Anderson HV, Roubin GS, Leimgruber PP, et al. Measurement of transstenotic pressure gradient during percutaneous transluminal coronary angioplasty. *Circulation* 1986; 73(6):1223-1230.
43. Rajabi-Jaghargh E, Kolli KK, Back LH, Banerjee RK. Effect of guidewire on contribution of loss due to momentum change and viscous loss to the translesional pressure drop across coronary artery stenosis: an analytical approach. *Biomed Eng Online* 2011; 10:51.
44. Ballyk PD, Steinman DA, Ether CR. Simulation of non-Newtonian blood flow in an end-to-end anastomosis. *Biorheology* 1994; 31(5):565-586.
45. Castro MA, Putman CM, Cebal JR. Computational fluid dynamics modeling of intracranial aneurysms: effects of parent artery segmentation on intra-aneurysmal hemodynamics. *Am J Neuroradiol* 2006; 27: 1703-1709.

## Figure legends

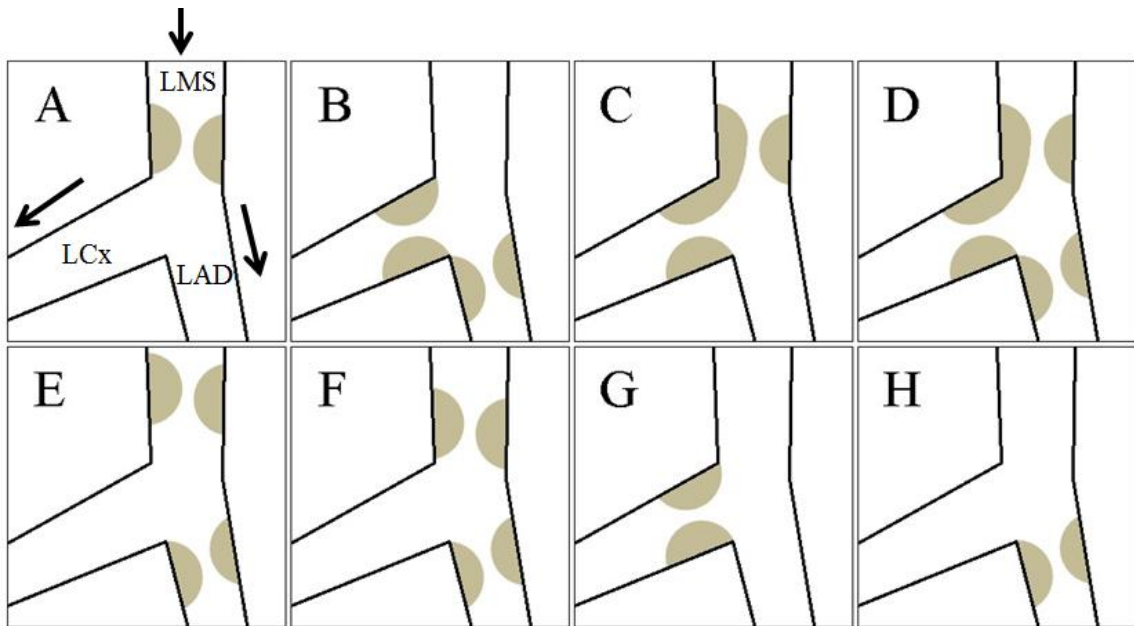


Figure 1. Diagram showing characterization of the eight types of bifurcation plaques in the left coronary artery. LMS-left main stem, LCD-left anterior descending, LCx-left circumflex.

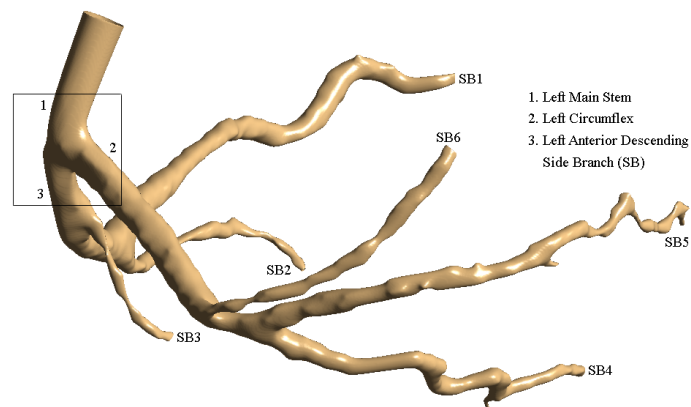


Figure 2. Realistic coronary model showing left coronary artery and its side-branches. The rectangle shows the effective plaque locations where eight types of bifurcation plaques are simulated to demonstrate hemodynamic variations.

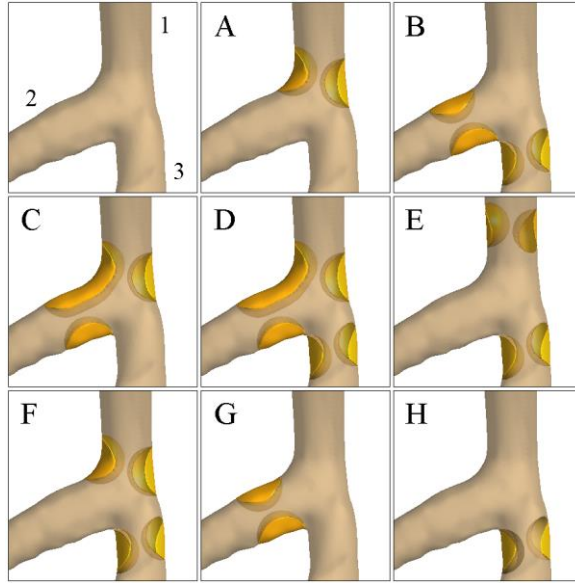


Figure 3. The realistic bifurcation plaques were simulated at different anatomical locations according to the diagram in Fig. 1.

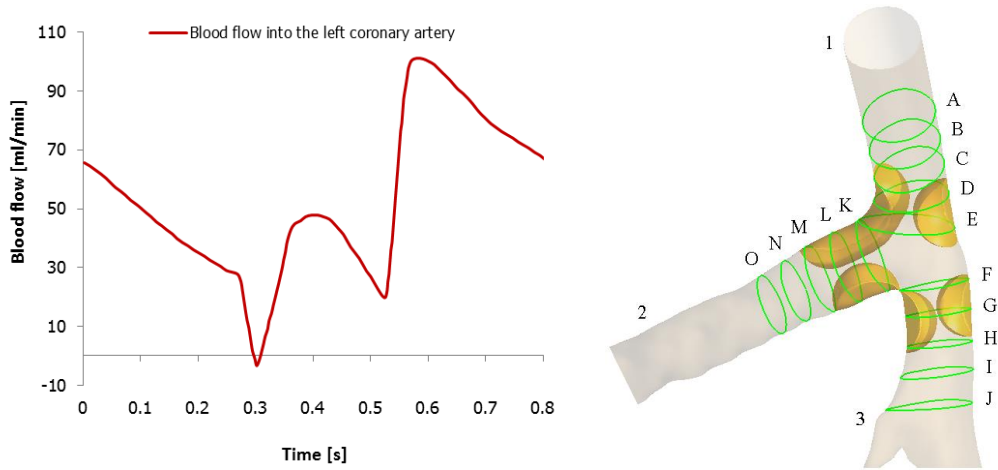


Figure 4. Pulsatile flow cycle into the left coronary artery (a). The fifteen cross-sections were defined to calculate the average velocity inside coronary bifurcation at effective plaque locations (b).

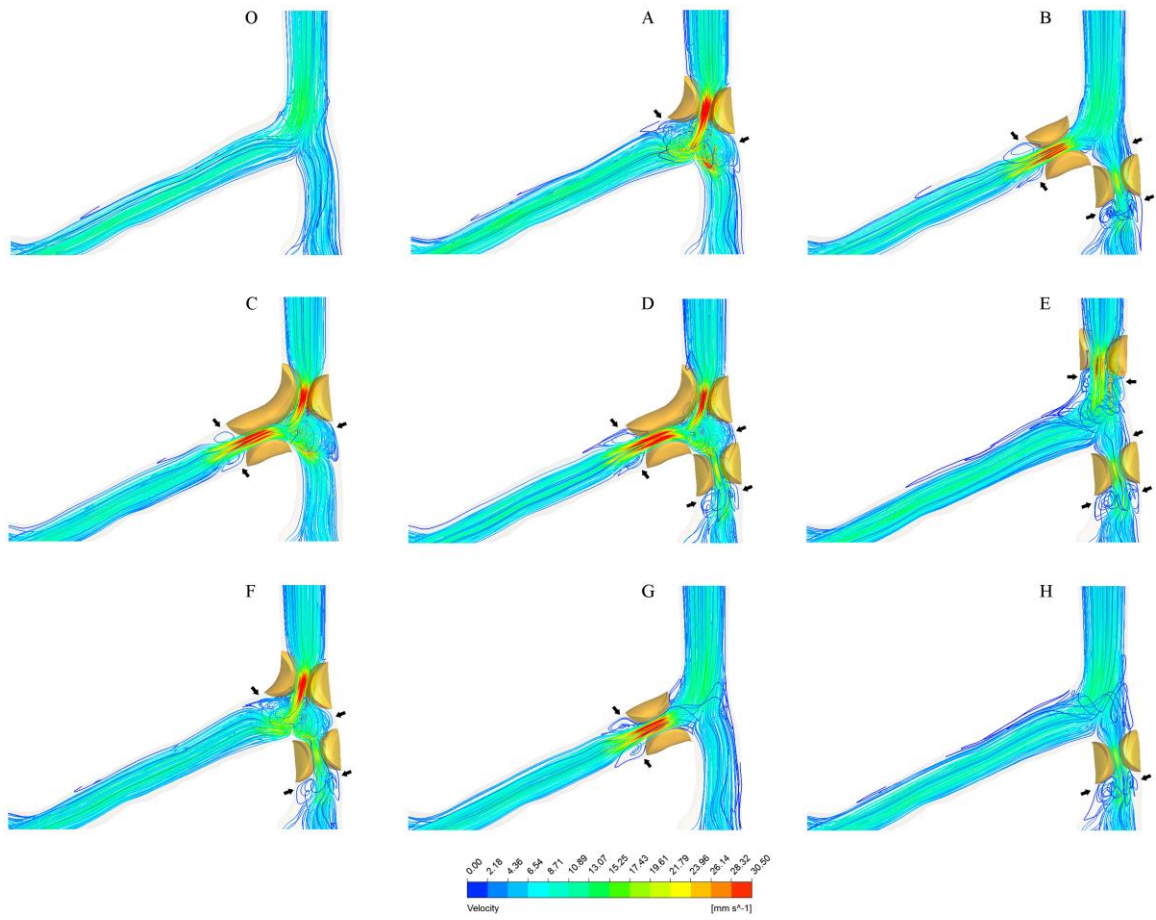


Figure 5. The velocity patterns inside left bifurcation at effective plaque locations with eight types of bifurcation plaques and normal condition during the systolic phase (0.2 s).

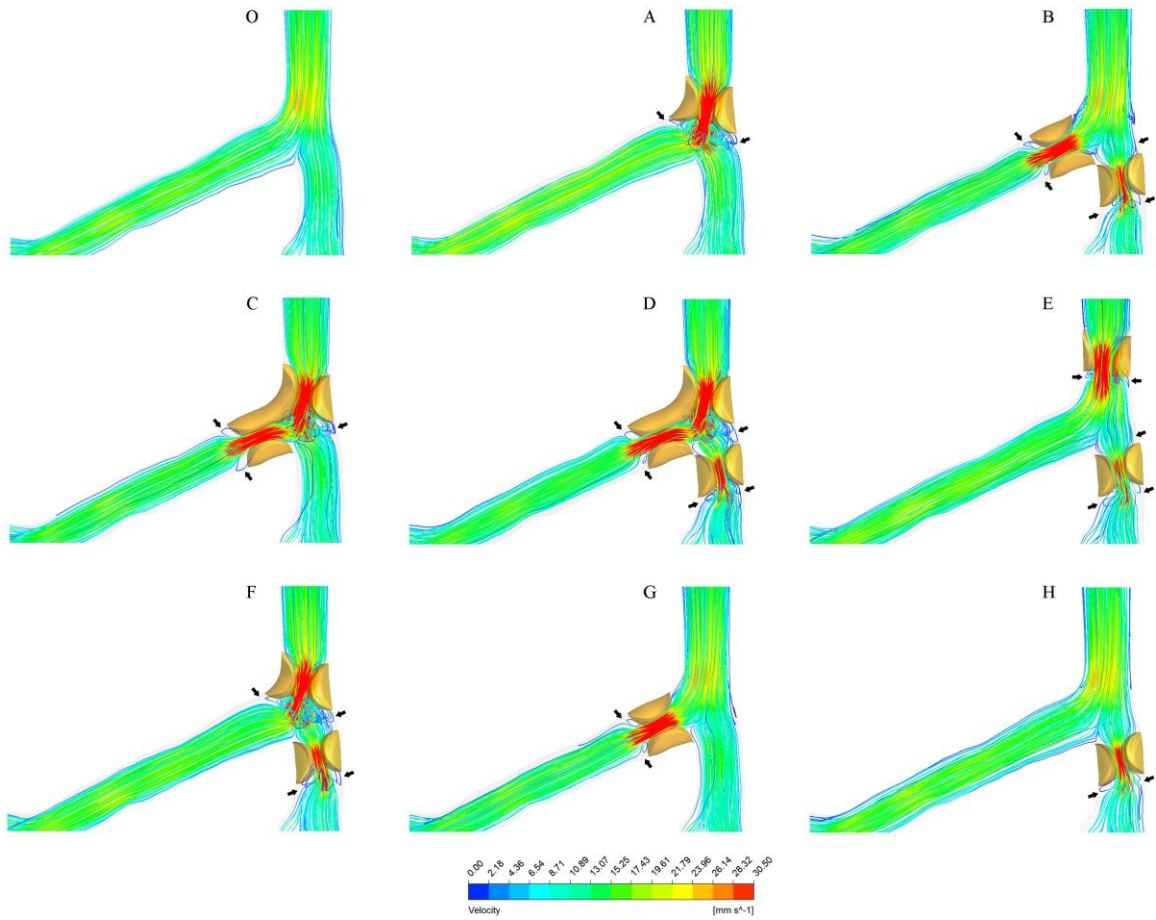


Figure 6. The velocity patterns inside left bifurcation at effective plaque locations with eight types of bifurcation plaques and normal condition during the diastolic phase (0.7 s).

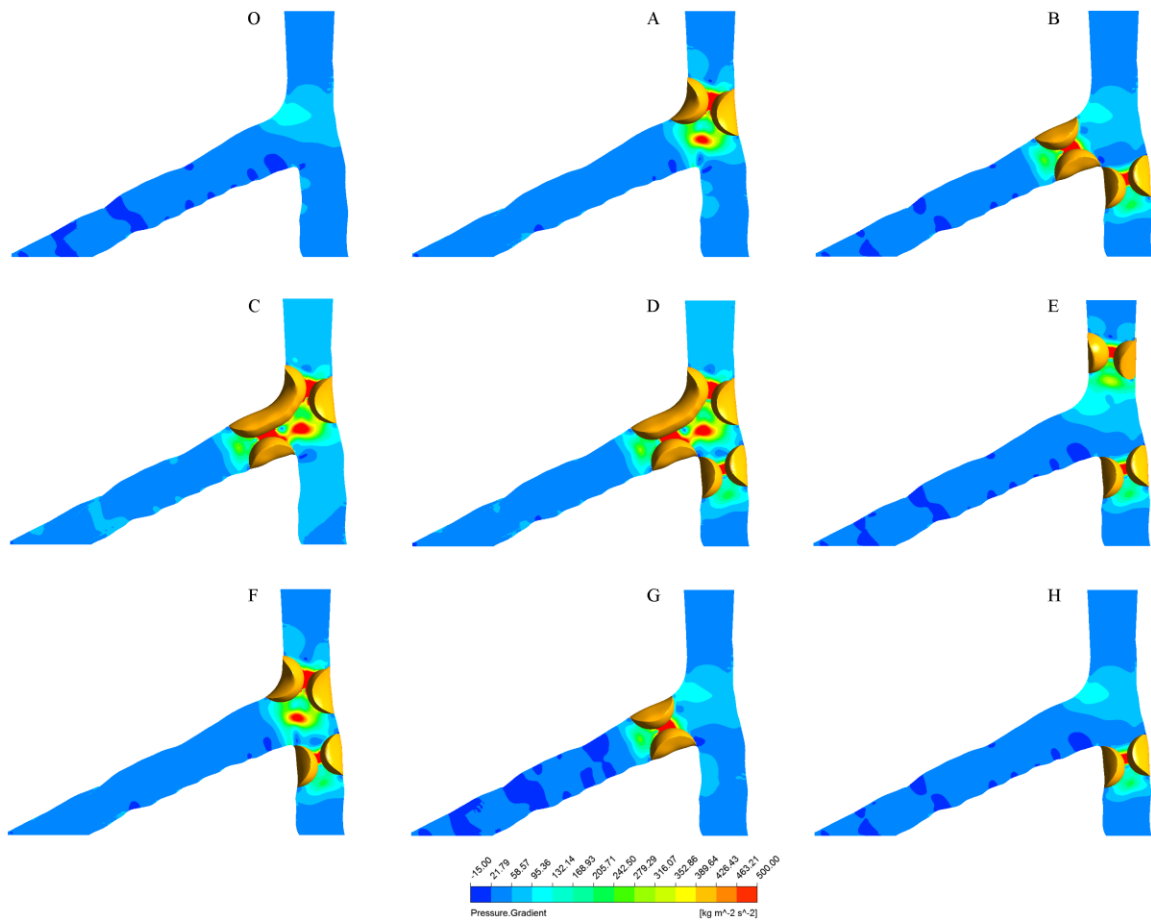


Figure 7. The pressure gradient patterns inside left bifurcation at effective plaque locations with eight types of bifurcation plaques and normal condition during the diastolic phase (0.7 s).

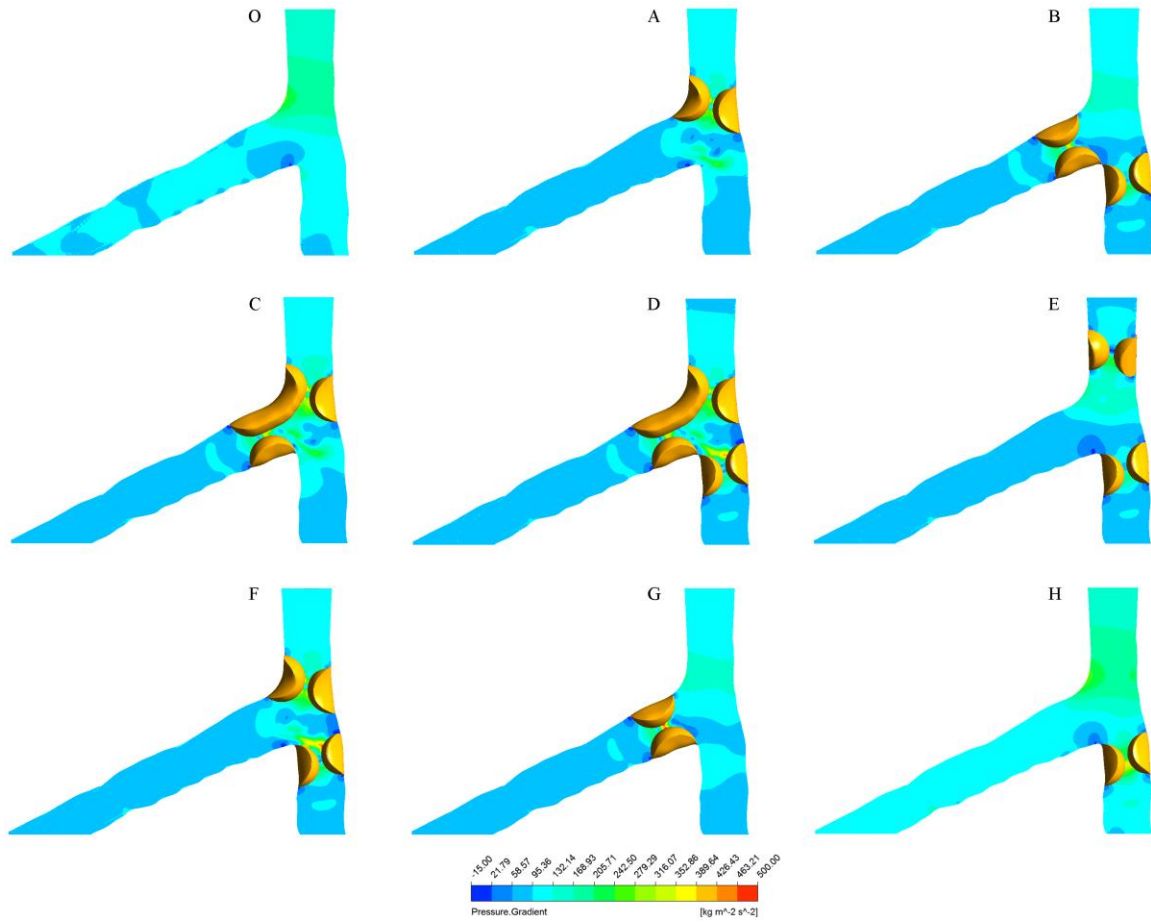


Figure 8. The pressure gradient patterns inside left bifurcation at effective plaque locations with eight types of bifurcation plaques and normal condition during the systolic phase (0.2 s).